Results in Chemistry 4 (2022) 100600

Contents lists available at ScienceDirect

Results in Chemistry

journal homepage: www.sciencedirect.com/journal/results-in-chemistry

Synthesis, crystal structure, exploration of the supramolecular assembly through Hirshfeld surface analysis and bactericidal activity of the cadmium organometallic complexes obtained from the heterocyclic ligand

Rizvan Kamil Askerov [a,*], Muhammad Ashfaq [b,*], Evgeny Vadimovich Chipinsky [c], Vladimir Kimovich Osmanov [c], Muhammad Nawaz Tahir [b], Evgeny Vladimirovich Baranov [d], Georgy Konstantinovich Fukin [d], Viktor Nikolaevich Khrustalev [e], Rovshan Hafiz Nazarov [f], Galina Nikolaevna Borisova [c], Zhanna Vladimirovna Matsulevich [c], Abel Mammadali Maharramov [a], Aleksandr Vladimirovich Borisov [c]

[a] Baku State University, Baku, Azerbaijan
[b] Department of Physics, University of Sargodha, Sargodha 40100, Pakistan
[c] Nizhny Novgorod State Technical University, Nizhny Novgorod, Russia
[d] Razuvaev Institute of Organometallic Chemistry, Russian Academy of Sciences, Nizhny Novgorod, Russia
[e] Peoples' Friendship University of Russia, Moscow, Russia
[f] Institute of Chemistry of Additives, Baku, Azerbaijan

ARTICLE INFO

Keywords:
1-(2-Chlorophenyl)-1,4-dihydro-5*H*-tetrazole-5-thione
1-(2-Methoxyphenyl)-1,4-dihydro-5*H*-tetrazole-5-thione
Polymeric cadmium(II) complexes
Crystal structure
Supramolecular assembly
Bactericidal activity

ABSTRACT

New complex compounds **(I-III)** were synthesized by successive reactions of sodium 1-(2-chlorophenyl)-1H-tetrazole-5-thiolate (**NaL^1**) with cadmium chloride and dimethyl sulfoxide or o-phenanthroline. Successive reactions of sodium 1-(2-methoxyphenyl)-1H-tetrazole-5-thiolate (**NaL^2**) with cadmium chloride and o-phenanthroline gave complexes **(IV, V)**. The structure of the obtained compounds was studied by ^{1}H, ^{13}C NMR, UV–vis spectroscopy and elemental analysis. Moreover, the crystal structure of complexes **(I-III/V)** was determined by the single crystal X-ray diffraction analysis. The supramolecular assembly was explored through Hirshfeld surface analysis in terms of strong as well as comparatively weak non-covalent interactions. The crystal packing environment of the non-polymeric crystal structures **(II/III/V)** was further explored by finding the interaction energy between the molecular pairs and energy frameworks. The ligands and the complexes were screened for their bactericidal activity against *Staphylococcus aureus* and *Escherichia coli.*

Introduction

N-Substituted mercaptotetrazoles and other five-membered heterocyclic thiols containing a nitrogen atom next to the C-SH group can exist both in thiol **(a)** and thione **(b)** forms due to tautomerism (Scheme 1) [1–4]. However, it is believed that the thionic form is more stable for mercaptotetrazoles and other similar heterocyclic compounds [1]. In addition, in the presence of bases, they can form thiolate anions **(c)**, which can be considered as a 6π-electron ring system, isoelectronic to the cyclopentadienyl anion. Possessing several electron donor centers, such forms of reagents can be used as polydentate ligands in complexation reactions with various metals in order to obtain various complexes and supramolecular structures (d-g) [2,3,5–15].

Earlier in works [2,5,15,16], the reactions of 1-phenyl-1,4-dihydro-5H-tetrazole-5-thione, 1-(4-fluorophenyl)-1,4-dihydro-5H-tetrazole-5-thione, 1-(2-fluorophenyl)-1,4-dihydro-5H-tetrazole-5-thione, 1-(2-methoxyphenyl)-1,4-dihydro-5H-tetrazole-5-thione, 1-(4-methoxyphenyl)-1,4-dihydro-5H-tetrazole-5-thione, 1-(2-methylphenyl)-1,4-dihydro-5H-tetrazole-5-thione and 1-(2-chlorophenyl)-1,4-dihydro-5H-tetrazole-5-thione with cadmium chloride were studied, and the structures of the obtained complexes were established by X-ray diffraction analysis. In [3] the structure of the reaction product of sodium 1-(2-methoxyphenyl)-1H-tetrazole-5-thiolate with cadmium chloride is presented.

* Corresponding authors.
E-mail addresses: rizvankam@bk.ru (R.K. Askerov), ashfaq.muhammad@uos.edu.pk (M. Ashfaq).

https://doi.org/10.1016/j.rechem.2022.100600
Received 1 September 2022; Accepted 20 October 2022
Available online 25 October 2022

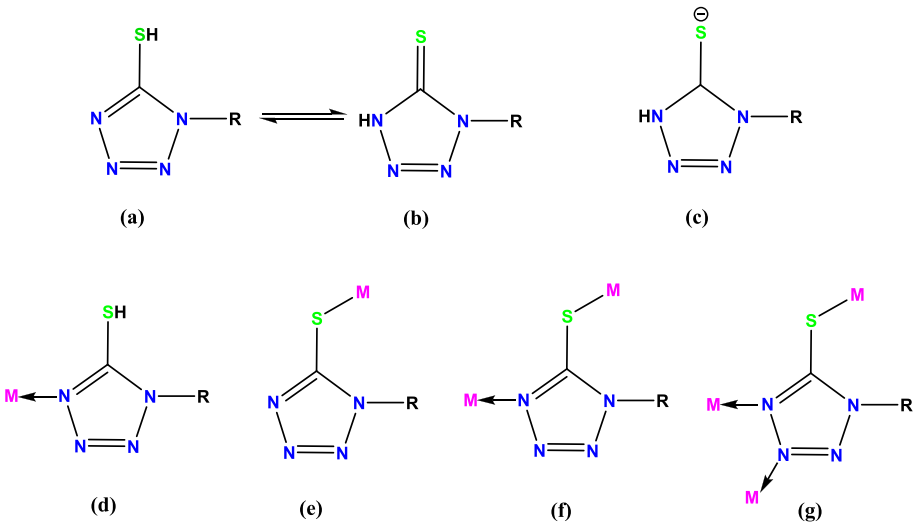

Scheme 1. Forms of *N*-substituted mercaptotetrazoles **(a-c)** and methods of their coordination with metal atoms **(d-g)**.

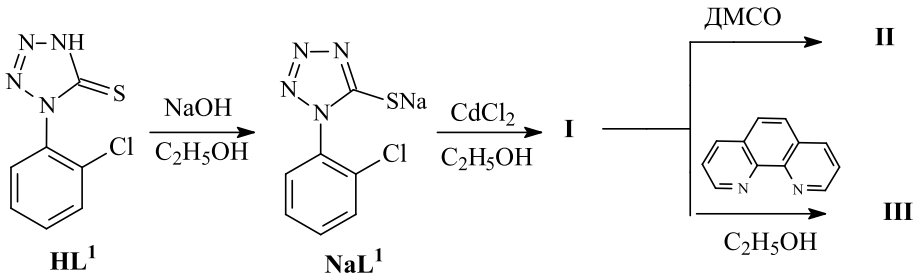

Scheme 2. Synthesis of complexes **I, II** and **III**.

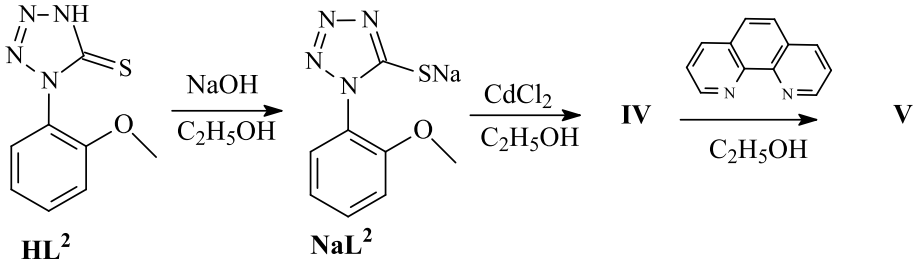

Scheme 3. Synthesis of complexes **IV** and **V**.

In this work, which is a continuation of our studies begun in [2,3,15,16], we studied the structure of the complex **I** - product of the reaction of cadmium chloride with sodium 1-(2-chlorophenyl)-1H-tetrazole-5-thiolate (NaL^1), as well as the structure of mixed complexes **II** and **III** obtained by the interaction of this product with dimethyl sulfoxide and o-phenanthroline (Scheme 2). For comparison, we studied the structure of mixed complex **V** obtained in the reaction of described in product of the reaction of sodium 1-(2-methoxyphenyl)-1H-tetrazole-5-thiolate with cadmium chloride **IV** with o-phenanthroline (Scheme 3).

The crystal structure of complex **I** is polymeric whereas the crystal structure of complex **II, III** and **V** is non-polymeric. Hirshfeld surface analysis is an excellent way to elaborate the non-covalent interactions in the crystal packing of the single crystals. The non-covalent interactions are the main source to predict the properties of the single crystals. Void analysis in single crystals is important to explore as the properties of single crystals specially the physical properties like melting point, mechanical strength etc depends on how much strongly the molecules are packed. In continuation our research work on the single crystal X-rays diffraction and Hirshfeld surface analysis of the complexes [17–22], here we are going to explore the synthesis, crystal structure, Hirshfeld surface analysis, enrichment ratio, void analysis and bactericidal activity of complexes **I-III** and **V**. The output file of single crystal X-rays diffraction is used for the Hirshfeld surface analysis, enrichment ratio calculations and void analysis.

Experimental

Material and methods

The following reagents NaN_3, $CdCl_2$, o-chlorophenylisothiocyanate (Acros Organics, Belgium) were used without additional purification. All melting points were determined with a “Stuart SMP3” melting point

Table 1
Basic crystallographic data and refinement parameters for compounds **I-III/V**.

Parameters	I	II	III	V
Empirical formula	$C_{14}H_8CdCl_2N_8S_2$	$C_{36}H_{40}Cd_2Cl_4N_{16}O_4S_8$	$C_{52}H_{32}Cd_2Cl_4N_{20}S_4$	$C_{56}H_{44}Cd_2N_{20}O_4S_4$
M	535.71	1383.92	1431.84	1414.17
Temperature, K	296(2)	296(2)	100(2)	100(2)
Crystal size, mm^3	0.38 × 0.06 × 0.03	0.33 × 0.17 × 0.13	0.30 × 0.25 × 0.02	0.30 × 0.25 × 0.02
Crystal system	Monoclinic	Triclinic	Triclinic	Triclinic
Space group	*C*2/*c*	*P*-1	*P*-1	*P*-1
a, Å	28.3131 (19)	9.0006(7)	10.0636 (17)	11.1462(2)
b, Å	8.7907 (6)	11.4534(9)	12.149 (4)	14.3981(3)
c, Å	7.5137 (5)	15.0039(12)	12.198 (4)	20.2381(4)
α, deg	90	108.042(1)	80.120 (13)	78.119(1)
β, deg	96.633 (2)	107.410(1)	9.969 (10)	88.325(1)
γ, deg	90	95.918(1)	84.841 (15)	67.516(1)
V, $Å^3$	1857.6 (2)	1370.23(19)	1379.7 (7)	2932.32(10)
Z	4	1	1	2
ρ_{calcd} g/cm^3	1.916	1.677	1.723	1.602
μ, mm^{-1}	1.706	1.329	1.175	0.933
F(000)	1048	692	712	1424
Data collection range over θ, deg	26	27	25	27
Measured reflections	1745	12,433	11,339	64,215
Independent reflections	1745	5935	4952	12,802
Number of refined parameters	113	442	371	788
R_1 ($I > 2\sigma(I)$)	0.061	0.046	0.112	0.021
w*R*2 (all data)	0.179	0.120	0.243	0.053
GOOF	1.12	1.08	1.40	1.03
Residual electron density (Δρmin/Δρmax), e $Å^{-3}$	−1.21/1.35	−0.97/1.03	−1.09/3.23	−0.51/0.72

apparatus and reported as such. The UV–vis spectra compounds were measured on an "Shimadzu UV-1800" (operating spectral range 190–1100 nm, wavelength error 0.1 nm), using a 1 cm path length cell in 96 % ethanol at room temperature. The concentration of substances in the solution is 10^{-4}M. The ^{1}H NMR spectra compounds were measured on an "Agilent DD2 400" spectrometer at 400.0 0 MHz, using DMSO- d6 as the NMR solvents. The ^{13}C NMR and DEPT spectra compounds were measured on an "Agilent DD2 400" spectrometer at 100.60 MHz, using DMSO- d6 as the NMR solvents. Chemical shifts are indicated in parts per million (ppm) relative to tetramethylsilane as an internal standard.

Synthesis of 1-(2-[chlorophenyl)-1,4-dihydro-5H-tetrazole-5-thion (HL1)

2-Chlorphenyl isothiocyanate (6.431 g, 39 mmol) was added to a solution of NaN_3 (2.53 g, 39 mmol) in H_2O (50 ml) at 20 °C. The reaction mixture was refluxed for 2 h, cooled to 20 °C, and filtered to remove non-dissolved impurities. A 10 % aqueous solution of HCl was added with stirring to the obtained solution to pH = 2. The precipitate formed was filtered off, washed with water (200 ml), and dried at 353 K. Yield 68 % as white powder, m.p. 434 K (with decomp.). Analysis calculated for $C_7H_5ClN_4S$ (%): C 39.53, H 2.37, N 26.35. Found (%): C 39.62, H 2.26, N 26.44. ^{1}H NMR (400.00 MHz, DMSO-d_6), δ ppm, (*J*, Hz): 7.75 (m, 2H, Ar); 7.67 (m, 1H, Ar); 7.59 (m, 1H, Ar). ^{13}C NMR (100.60 MHz, DMSO-d_6), δ ppm: 159.60 (C═S); 135.44 (C—N, Ar); 131.48 (C—Cl, Ar); 131.20, 131.01, 130.43, 128.11 (CH, Ar).

Synthesis of complex (I)

A solution of thione **(HL^1)** (2 mmol) in 95 % ethanol (15 ml) was added to a solution (2 mmol) sodium hydroxide in 95 % ethanol (15 ml), and then added a solution of $CdCl_2$ (1 mmol) in 95 % ethanol (15 ml). The reaction mixture was kept for 168 h at 293 K, the precipitated precipitate of compound (**I**) was filtered, washed with 50 ml of ethanol and dried at 353 K. The substance for X-ray study was used without additional recrystallization. Yield 55 % as white powder, m.p. 463 K (with decomp.). Analysis calculated for $C_{14}H_8CdCl_2N_8S_2$ (%): C 31.40, H 1.49, N 20.93 Found (%): C 31.49, H 1.44, N 20.84. ^{1}H NMR (400.00 MHz, DMSO-d_6), δ (ppm): 7.72 (d,1H, Ar), 7.56 (m, 3H, Ar). ^{13}C NMR (100.60 MHz, DMSO-d_6), δ ppm: 163.23 (C—S—Cd); 133.31 (C—N, Ar); 132.27 (CH, Ar); 131.26 (C—Cl, Ar); 130.73, 130.34, 128.64 (CH, Ar).

Synthesis of complex (II)

Yield 22 % as white powder, m.p. 458 K (with decomp.). Analysis calculated for $C_{36}H_{40}Cd_2Cl_4N_{16}O_4S_8$ (%): C 31.25, H 2.89, N 16.20. Found (%): C 31.30H 2.98, N 16.11. ^{1}H NMR (400.00 MHz, DMSO-d_6), δ ppm: 7.71(d., 1H, *J* = 8.0 Hz, Ar); 7.57 (m, 3H, Ar); 2.48 (m, $(CH_3)_2SO$). ^{13}C NMR (100.60 MHz, DMSO-d_6), δ ppm: 162.87 (C—S—Cd); 133.26 (C—N, Ar); 132.33 (CH, Ar); 131.23 (C—Cl, Ar); 130.73, 130.33, 128.69 (CH, Ar); 40.86 ($2CH_3$, $(CH_3)_2S$=O).

Synthesis of complex (IV)

The complex (**IV**) used in the work was obtained and described in [3]. ^{1}H NMR (400.00 MHz, DMSO-d_6), δ (ppm): 7.52 (M., 1H, Ph), 7.33 (д.д., 1H, *J* = 7.2, 1.6 Гц, Ph), 7.24(д., 1H, *J* = 8.5 Гц, Ph), 7.07 (M., 1H, Ph), 3.73 (c., 3H, OCH_3). ^{13}C NMR (100.60 MHz, DMSO-d_6), δ (ppm): 162.72 (C—S—Cd), 154.81 (C—OCH3, Ar), 131.99 (CH, Ar), 129.16 (CH, Ar), 124.17 (C—N, Ar), 120.90 (CH, Ar), 113.31 (CH, Ar), 56.32 (O—CH_3).

Synthesis of complexes (III) and (V)

A solution of o-phenanthroline (1 mmol) in dry ethanol (5 ml) was added to a boiling solution (1 mmol) of complex (**I**) or (**IV**) in dry ethanol (100 ml). The reaction mixture was boiled for 5 h and the resulting precipitate was filtered directly from the hot solution. The crystals obtained were used for XRD analysis without additional recrystallization.

Yield of complex (III)

The yield of complex **III** is 62 % as white powder, m.p. 484 K (with decomp.). Analysis calculated for $C_{52}H_{32}Cd_2Cl_4N_{20}S_4$ (%): C 43.63, H

Table 2
Selected bond lengths (Å) and bond angles (°) in complexes **I-III/V**. Symmetry codes are: (i) − x, y, −z + 3/2; (ii) − x, −y + 1, −z + 2; (iii) ×, −y + 1, z − 1/2; (iv) − x + 1, −y + 2, −z + 1; (v) − x + 1, −y + 1, −z + 1; (vi) − x, −y + 2, −z.

Selected bond lengths in complex **I**					
Cd1-N1	2.224 (10)	Cd1—S1^{ii}	2.493 (3)	Cd1—S1^{iii}	2.493 (3)
Cd1-S1	2.493 (3)				
Selected bond angles in complex **I**					
N1^{i}-Cd1-N1	101.9 (6)	N1^{i}-Cd1-S1^{iii}	116.0 (3)	N1-Cd1-S1^{iii}	108.7 (3)
N1^{i}-Cd1-S1^{ii}	108.7 (3)	N1-Cd1-S1^{ii}	116.0 (3)	S1^{ii}-Cd1-S1^{iii}	105.96 (15)
Selected bond lengths in complex **II**					
Cd1-O1	2.315 (3)	Cd1-O2^{iv}	2.445 (3)	Cd1-S2	2.5790 (12)
Cd1-N1	2.405 (3)	Cd1-O2	2.414 (3)	Cd1-S1^{iv}	2.5886 (11)
Selected bond angles in complex **II**					
O1-Cd1-N1	91.50 (13)	O2-Cd1-S2	167.12 (8)	O1-Cd1-S1^{iv}	101.49 (10)
O1-Cd1-O2	85.26 (10)	O2^{iv}-Cd1-S2	92.96 (7)	N1-Cd1-S1^{iv}	159.33 (8)
N1-Cd1-O2	78.52 (11)	O2-Cd1-O2^{iv}	82.85 (10)	O2-Cd1-S1^{iv}	86.52 (8)
O1-Cd1-O2^{iv}	165.02 (11)	O1-Cd1-S2	96.66 (7)	O2^{iv}-Cd1-S1^{iv}	86.89 (8)
N1-Cd1-O2^{iv}	77.24 (11)	N1-Cd1-S2	88.68 (9)	S2-Cd1-S1^{iv}	105.48 (4)
Selected bond lengths in complex **III**					
Cd1-N4^{v}	2.321 (15)	Cd1-S2	2.566 (4)	Cd1-N9	2.465 (13)
Cd1-N10	2.343 (12)	Cd1-S1	2.574 (4)		
Selected bond angles in complex **III**					
N4^{v}-Cd1-N10	96.8 (4)	N9-Cd1-S2	169.5 (3)	N10-Cd1-S1	131.9 (3)
N4^{v}-Cd1-N9	84.4 (4)	N4^{v}-Cd1-S1	120.4 (3)	N9-Cd1-S1	82.4 (3)
N10-Cd1-N9	71.3 (4)	N10-Cd1-S2	98.3 (3)	S2-Cd1-S1	104.72 (14)
N4^{v}-Cd1-S2	98.1 (3)				
Selected bond lengths in complex **V**					
Cd1-N5	2.3143 (14)	Cd2-N18	2.3021 (13)	Cd2-N20	2.4049 (13)
Cd1-N10	2.3617 (13)	Cd2-N19	2.3775 (13)	Cd2-S3	2.5760 (4)
Cd1-N9	2.4496 (13)	Cd1-S1	2.5778 (4)	Cd2-S4^{vi}	2.5819 (4)
Cd1-S2^{v}	2.5658 (4)				
Selected bond angles in complex **V**					
N5-Cd1-N10	94.35 (5)	N18-Cd2-N19	85.28 (5)	N19-Cd2-S3	161.00 (3)
N5-Cd1-N9	83.93 (5)	N18-Cd2-N20	94.52 (5)	N20-Cd2-S3	92.40 (3)
N10-Cd1-N9	69.36 (5)	N19-Cd2-N20	69.91 (4)	N18-Cd2-S4^{vi}	106.27 (3)
N5-Cd1-S2^{v}	105.58 (3)	N18-Cd2-S3	103.55 (3)	N19-Cd2-S4^{vi}	91.50 (3)
N10-Cd1-S2^{v}	146.62 (3)	N9-Cd1-S1	165.66 (3)	N20-Cd2-S4^{vi}	151.01 (3)
N9-Cd1-S2^{v}	86.15 (3)	S2^{v}-Cd1-S1	105.040 (13)	S3-Cd2-S4^{vi}	101.835 (13)
N5-Cd1-S1	101.22 (3)	N10-Cd1-S1	96.76 (3)		

2.23, N 19.58. Found (%): C 43.68, H 2.14, N 19.63. ^{1}H NMR (400.00 MHz, DMSO-d_6), δ (ppm): 9.14 (bs.,2H, phen), 8.83 (d., 2H, J = 8.4 Hz, phen), 8.23 (s., 2H,phen), 8.05 (m., 2H, phen), 7.64 (d., 2H, J = 7.6 Hz, Ar), 7.53 (m, 2H, Ar), 7.43 (m., 4H, Ar). ^{13}C NMR (100.60 MHz, DMSO-d_6), δ (ppm): 163.72 (C—S—Cd), 150.49 (2CH, phen), 140.52 (2C, phen), 139.93 (2CH, phen), 133.34 (C—N, Ar), 132.5 (CH, Ar), 131.25 (C—Cl, Ar), 130.67, 130.20 (CH, Ar), 129.26 (2C, phen), 128.51 (CH, Ar), 127.57 (2CH, phen), 125.64 (2CH, phen).

Yield of complex (V)

The yield of complex **V** is yield 68 % as white powder, m.p. 482 K (with decomp.). Analysis calculated for $C_{56}H_{44}Cd_2N_{20}O_4S_4$ (%): C 47.59, H 3.11, N 19.83. Found (%): C 47.68, H 3.06, N 19.92. ^{1}H NMR (400.00 MHz, DMSO-d_6), δ (ppm): 9.12 (bs.,2H, phen), 8.82 (d.d., 2H, J = 8.4, 0.8 Hz, phen), 8.22 (s., 2H,phen), 8.04 (m., 2H, phen), 7.44 (m., 2H, Ar), 7.16 (m, 4H, Ar), 6.96 (m., 2H, Ar).

^{13}C NMR (100.60 MHz, DMSO-d_6), δ (ppm): 163.21 (C—S—Cd), 154.76 (C—OCH3, Ar), 150.48 (2CH, phen), 140.62 (2C, phen), 139.83 (2CH, phen), 131.82 (CH, Ar), 129.22 (2C, phen), 128.98 (CH, Ar), 127.57 (2CH, phen), 125.59 (2CH, phen), 124.21 (C—N, Ar), 120.74, 113.25 (CH, Ar), 56.25 (O—CH_3).

Details of X-rays diffraction analysis of complexes (I-III/V)

X-ray diffraction analysis of compounds **I, III,** and **V** was obtained on a Bruker D8 QUEST diffractometer, for compound **II** - on a Bruker Smart Apex diffractometer (ω-scan, MoK$_\alpha$ radiation, λ = 0.71073 Å). Experimental sets of reflection intensities were collected and integrated using the SMART and SAINT programs, respectively. The structures were solved by a direct method and refined by full-matrix least squares in F^2_{hkl} in the anisotropic approximation for non-hydrogen atoms. It was found that in the crystal of compound **II,** the chlorophenyl fragment of the ligand (**L^1**) is disordered over three positions and one DMSO molecule over two positions with populations of 0.35: 0.49: 0.16 and 0.89: 0.11, respectively. In the crystal of compound **V**, one of the CH_3 groups of the ligand (**L^2**) in molecules **A** and **B** is disordered over two positions with populations of 0.70: 0.30 and 0.75: 0.25, respectively. The coordinates of the remaining hydrogen atoms in **I, II, III,** and **V** were calculated from geometric considerations and refined with fixed positional ("rider" model) and thermal parameters (1.5U$_{iso}$ (C) for methyl groups (II and V) and U$_{iso}$ (H) = 1.2U$_{iso}$ (C) for all other groups). The structure was refined and absorption was taken into account using the SHELXTL and SADABS software packages. The crystal of compound **I** is a non-melohedral twin, the ratio of single-crystal components (domains) is ~ 62: 38 %. The structure of **I** was refined for two domains of the twin using the HKLF5 instruction. The crystallographic data and parameters of X-ray diffraction experiments of compounds **I, II, III,** and **V** are shown in Table 1. Selected bond lengths and bond angles are listed in Table 2. The structures are deposited in the Cambridge Structural Data Bank (CCDC) under the numbers 2100741 (**I**), 1869250 (**II**), 2100739 (**III**), 2044439 **(V)**.

Details related to bactericidity of compounds

Bactericidity of compounds (**HL^1, HL^2, I, IV**) was evaluated against the following bacteria: a Gram-positive strain of *Staphylococcus aureus* and a Gram-negative strain of *Escherichia coli*. The test compounds in the form of 1 % solutions in DMSO were placed in Petri dishes in wells with agarized medium of a beef-extract agar (D = 5 mm) and inoculated by a bacterial suspension prepared in a physiological solution (1 × 108 cells/

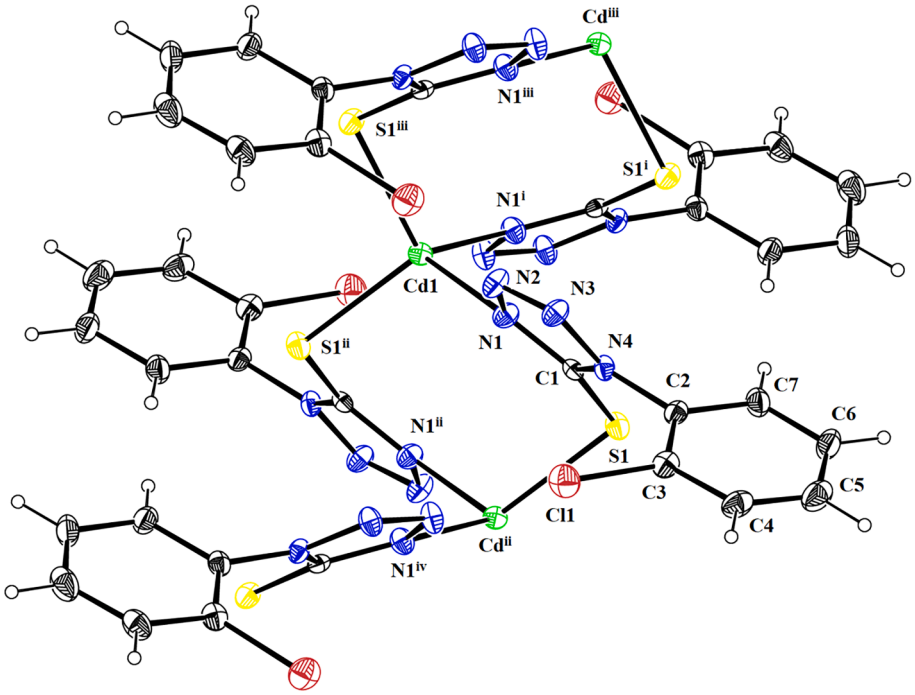

Fig. 1. ORTEP diagram of complex **I** that is drawn at probability level of 20%. H-atoms are shown by small circles of arbitrary radii.

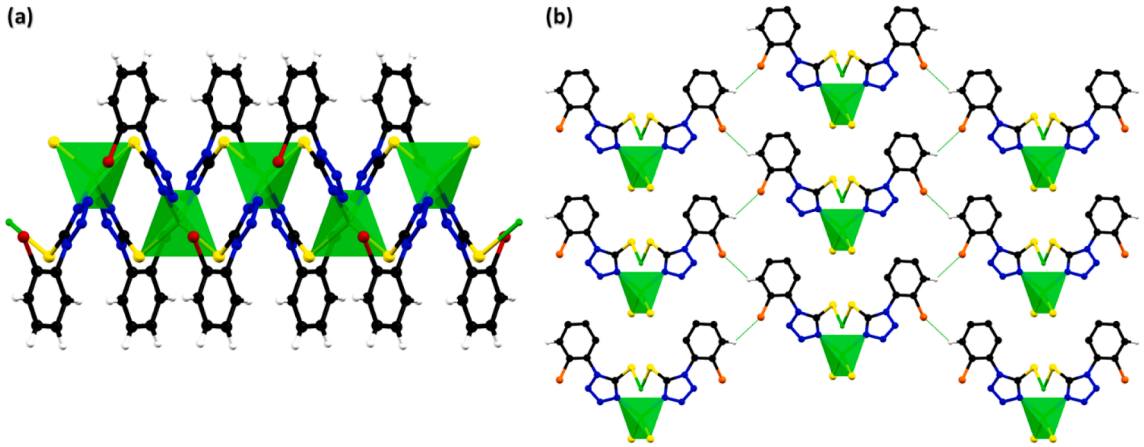

Fig. 2. (a) Polymeric chain of complex **I** that runs along c-axis. **(b)** Packing diagram of complex **I** showing the interlinkage of the neighbouring chains through H-bonding.

mL). Incubation was carried out in a thermostat at 37 °C for 24 h.

The degrees of bactericidity were estimated from the value of the growth inhibition zone of the test cultures formed around the wells with the studied compound. ^{1}H NMR spectroscopy showed that all compounds used were stable in DMSO-d_6 for 3 months at room temperature.

Details of theoretical study

The crystallographic information file (CIF) is used for performing the theoretical calculations. The interaction energy between molecular pairs and energy frameworks are calculated for the non-polymeric crystal structures (**II/III/V**) by using Crystal Explorer software version 21.5. Tonto program with HF/3-21G electron density model present in Crystal Explorer software is used for the calculations.

Results and discussion

Exploration of the crystal structure of complexes (I-III/V)

It was found by X-ray diffraction analysis that the reaction product of cadmium chloride with sodium 1- (2-chlorophenyl) −1H-tetrazole-5-thiolate Na**L**^{1} is a one-dimensional polymer complex with a chain structure of the composition $[Cd(\mu\text{-}L^1)_2]_n$, similar in structure complexes obtained in the reactions of 1-phenyl-1,4-dihydro-5H-tetrazole-5-thione, 1-(4-fluorophenyl)-1,4-dihydro-5H-tetrazole-5-thione and 1-(4-methoxyphenyl)-1,4-dihydro-5H-tetrazole-5-thione with cadmium chloride [2,15,16]. The structure-forming unit of the polymer complex is the Cd $(\mathbf{L}^1)_2$ fragment with two symmetric thionic ligands **L**^{1} (Fig. 1,

Table 3
Hydrogen bond geometry (°, Å) for complex **I-III/V.**

I	*D*—H···*A*	*D*—H	H···*A*	*D*···*A*	<(*D*—H···*A*)°
	C4—H4···Cl1^{i}	0.93	2.90	3.665 (7)	140
II	*D*—H···*A*	*D*—H	H···*A*	*D*···*A*	<(*D*—H···*A*)°
	C3*A*—H3*A*···S2^{ii}	0.93	2.96	3.823 (7)	154
	C17—H17*C*···O1	0.96	2.58	3.325 (9)	135
	C18—H18*A*···N5^{ii}	0.96	2.57	3.437 (8)	150
III	*D*—H···*A*	*D*—H	H···*A*	*D*···*A*	<(*D*—H···*A*)°
	C19—H19···N8^{iii}	0.95	2.58	3.442 (18)	151.82
	C20—H20···S1^{iii}	0.95	2.86	3.465 (14)	122
V	*D*—H···*A*	*D*—H	H···*A*	*D*···*A*	<(*D*—H···*A*)°
	C7—H7···N3^{iv}	0.95	2.45	3.395 (3)	174
	C8*A*—H8*C*···N7^{v}	0.98	2.59	3.428 (3)	144
	C15—H15···O1^{v}	0.95	2.63	3.353 (2)	134
	C15—H15···N4^{v}	0.95	2.67	3.331 (2)	127
	C16—H16*A*···S4^{v}	0.98	2.78	3.632 (2)	146
	C17—H17···S2^{v}	0.95	2.85	3.4761 (18)	124
	C26—H26···S1	0.95	3.01	3.6904 (17)	130
	C35—H35···N13^{vi}	0.95	2.62	3.510 (3)	157
	C36*A*—H36*B*···N16^{vii}	0.98	2.67	3.472 (3)	140
	C44—H44*C*···S2^{v}	0.98	2.95	3.5087 (18)	117
	C44—H44*C*···O2^{v}	0.98	2.61	3.359 (2)	133
	C45—H45···S4^{vii}	0.95	2.96	3.5988 (18)	126
	C54—H54···S3	0.95	2.94	3.6107 (17)	129

Symmetry codes: (i) $-x+1/2, y-1/2, -z+5/2$; (ii) $x-1, y, z$; (iii) $-x+1, -y+1, -z$; (iv) $-x+1, -y, -z+1$; (v) $-x+1, -y+1, -z+1$; (vi) $-x, -y+1, -z$; (vii) $-x, -y+2, -z$.

Table 1), which are linked by the C_2 rotational axis passing through the Cd (1) atom. Polymer chain of complex **I** is formed by the syndiotactic alternation of Cd $(\mathbf{L^1})_2$ fragments with Cd1^{i}, Cd1, Cd1^{ii}, Cd1^{iv} atoms, etc. along the crystallographic axis ***c*** (Fig. 2a). The coordination environment of the cadmium cation Cd (1) is a distorted tetrahedron, at the vertices of which there are two nitrogen atoms N (1), N1^{i} of two symmetric ligands $\mathbf{L^1}$ in the complex and two sulfur atoms S1^{ii}, S1^{iii} from two adjacent fragments Cd $(\mathbf{L^1})_2$ A and B in the chain. The Cd(1)- N(1)and Cd (1) - S(1) distances are 2.224 (10) Å and 2.493 (3) Å and are close to similar bond lengths (2.228 (4) – 2.233 (3) Å and 2.497 (11) –2.506 (11) Å) in previously published complexes [2,15,16]. The 1D chains in the complexes contain an eight-membered cycle (—S—C═N → Cd—S—C═N → Cd) in the "chair" conformation. The polymer chains of complex **I** are interlinked through C—H···Cl bonding to form chains along a and b-axis (Table 3). So, a three dimensional network of polymers is formed through H-bonding. Only a small portion of each polymeric chains is shown in (Fig. 2b) for clarity because the main focus is to show the interlinkage of the neighbouring chains through H-bonding. The crystal packing of complex **I** is further stabilized by weak off-set π···π stacking interactions between the five and six-membered rings of the symmetry related chains with inter-centroid separation ranges from 3.758 (9) to 4.281 (7) Å. Ring off-set for interacting rings range from 1.694 to 1.703 Å.

At the same time, product **IV**, obtained by us earlier in the reaction of sodium 1-(2-methoxyphenyl)-1H-tetrazole-5-thiolate Na$\mathbf{L^2}$ with cadmium chloride, is a one-dimensional polymer complex with a chain structure of the composition $[Cd(\mu\text{-}\mathbf{L^2})_2]_n$, in which the 1D-chains in the complexes contain an eight-membered ring with a different sequence of atoms in the cycle (—S —C═N → Cd ← N═C—S—Cd) in the "bath" conformation [3].

By recrystallization of complex **I** from dimethyl sulfoxide, a new

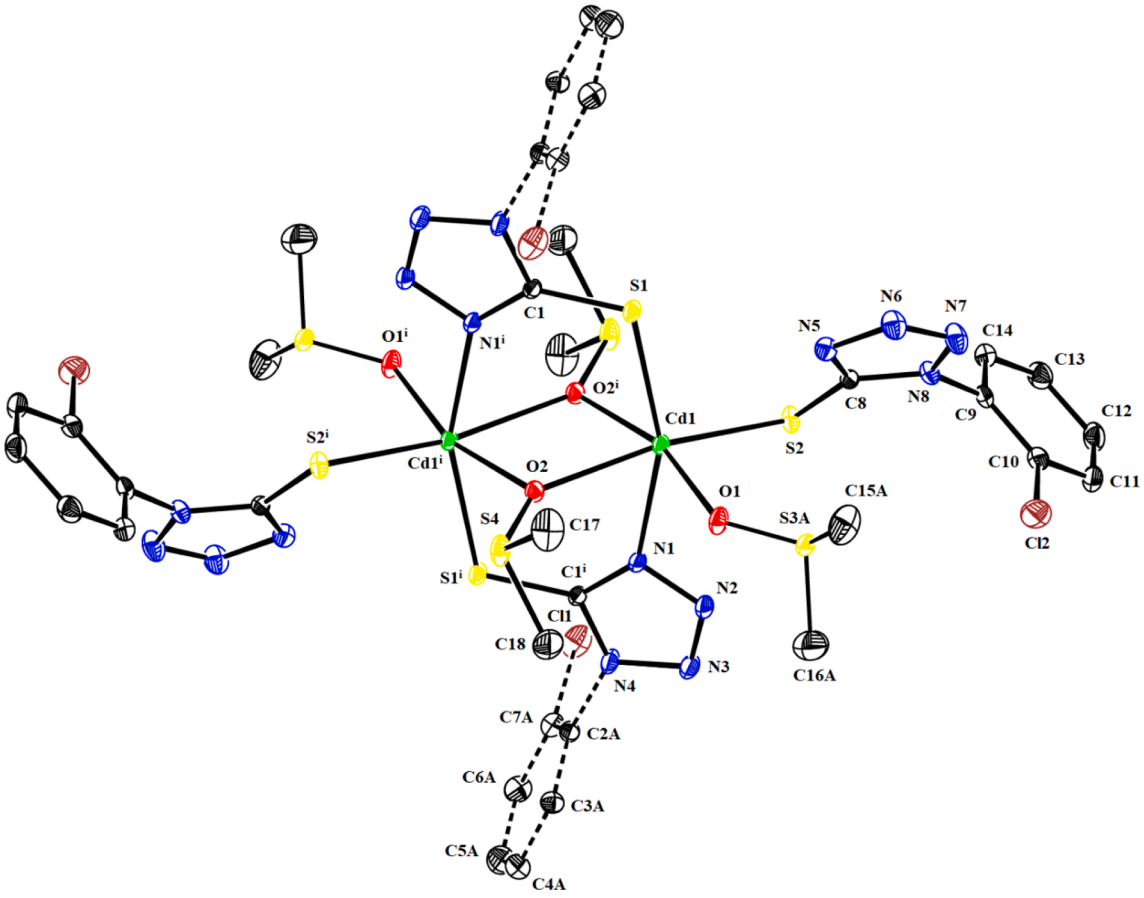

Fig. 3. ORTEP diagram of complex **II** that is drawn at probability level of 10%. H-atoms are not shown for clarity.

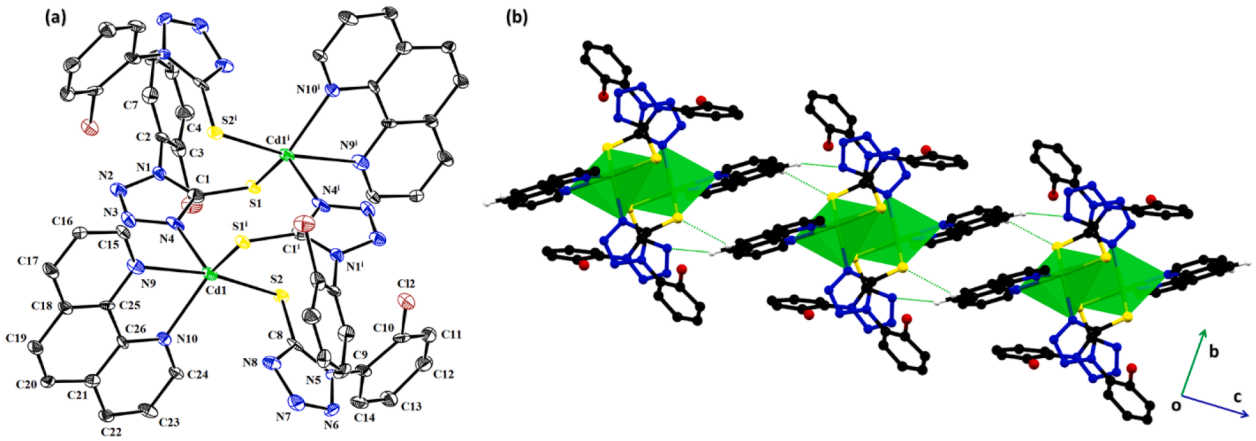

Fig. 4. **(a)** ORTEP diagram of complex **III** that is drawn at probability level of 20%. H-atoms are not shown for clarity. **(b)** Packing diagram of complex **III** viewed along a-axis.

complex **II** of molecular structure was obtained (Fig. 3). Compound **II** is a binuclear complex with the composition $[Cd_2(\mu\text{-}\mathbf{L^1})_2(\mathbf{L^1})_2(\mu\text{-}DMSO)_2(DMSO)_2]$. The coordination polyhedron of the cadmium (II) atom is a distorted octahedron with O (1), O (2), O (2A), and S (1) atoms in the equatorial plane, N (1) and S (2) atoms in axial positions. The Cd (1)—N (1) and Cd (1)—S (2) distances are 2.405 (3) Å and 2.5790 (12) Å and are close to similar bond lengths in previously published polymer-type complexes (2.338 (2)–2.459 (2) Å and 2.569 (7)–2.574 (9) Å) [4]. Complex **II** has its own symmetry Ci: the inversion center is located in the center of a rhombus consisting of O (2), O (2^i), Cd (1), Cd (1^i) atoms and coincides with the crystallographic inversion center of the crystal. The Cd (1)—Cd (1^i) distance in complex (**II**) is 3.643 (4) Å. The distances Cd (1)—O (1), Cd (1)—O (2), Cd (1)—O (2^i), and Cd (1)—S (1) are 2.315 (3) Å, 2.414 (3) Å, 2.445 (3) Å, and 2.589 (1) Å, respectively. The molecular configuration is stabilized by intra molecular C—H···O bonding. The moelcules are interlinked through C—H···S and C—H···N bonding as shown in Fig. S1. The further stabilization of the crystal packing is due to C—H···π interaction with H···π distance ranges from 2.96 to 3.87 Å.

By boiling complex **I** with o-phenanthroline in absolute ethanol, binuclear complex **III** of composition $[Cd_2(\mu\text{-}\mathbf{L^1})_2(\mathbf{L^1})_2(phen)_2]$ was obtained (Fig. 4a). The coordination polyhedron of the Cd (II) atom in **III** is seemed to be a distorted trigonal bipyramid. The basal plane is formed by one atom N(4) *phen* [Cd(1)-N(4) = 2.321 (15) Å)], atoms N(10) [Cd (1)-N(10) = 2.343 (12) Å] and S(1) [Cd(1)-S(1) = 2.574 (4) Å] from two ligands $\mathbf{L^1}$. The axial positions contain the second atom N (9) *phen* [Cd (1)-N(9) = 2.465 (13) Å] and atom S(2) [Cd(1)-S(2) = 2.566 (4) Å] from the third ligand $\mathbf{L^1}$. From this point of view, the geometric parameter $\tau = (\alpha\text{-}\beta)$ / 60 is applicable to 5-coordinate structures as an indicator of the distortion degree of the metal coordination sphere between trigonal - bipyramidal and tetragonal - pyramidal configurations. For an ideal tetragonal pyramid τ is equal to zero, and for an ideal trigonal bipyramid – 1.0.

In compound **III**, the largest angles between the cadmium substituents S (1), S (2), N (9), and N (10) are α = 169.5 (3)° for N (9) Cd (1) S (2) and β = 131.9 (3)° for N (10) Cd (1) S (1). Thus, τ is equal to (169.5–131.9)/60 = 0.63, indicating only 37 % of the contribution of the tetragonal pyramidal geometry. Thus, the cadmium ions in complex **III** are pentacoordinate, and the Cd (II) coordination polyhedron has an intermediate configuration close to the trigonal bipyramid. Complex **III** is centrosymmetric and contains an eight-membered cycle (–S–C═N → Cd–S–C═N → Cd) in the "chair" conformation; the center of the inversion is in the middle of the eight-membered cycle and coincides with the crystallographic center of the inversion. The Cd (1)–Cd (1A) distance in the cycle is equal to 4.101 (2) Å. The molecules are interlinked by C-H···N and C-H···S bonding to form infinite chain of molecules that runs along c-axis (Fig. 4b).

Although the structures of complex **I** and complex **IV** described in article are different, the reaction of complex **IV** with o-phenanthroline also leads to the formation of complex **V** of molecular structure. X-ray diffraction analysis of complex **V** showed that the single-crystal sample obtained after crystallization of the compound from ethyl alcohol contains two independent centrosymmetric molecules A and B of complex **V** (Fig. 5a). Molecule **A** and **B** looks identical, but these molecules are different with respect to each other as far as the crystallography is concerned. Compound **V** is a binuclear with the composition of $[Cd_2(\mu\text{-}\mathbf{L^2})_2(\mathbf{L^2})_2(phen)_2]$. The coordination polyhedron of the Cd (II) atom in **V** is a distorted octahedron, at the base of which the N (4) and N (10) atoms of two chelating molecules ($\mathbf{L^2}$ and phen) and two N (8A) and S (2) atoms from two molecules of ligand ($\mathbf{L^2}$) are located. The axial positions are occupied by the second atoms N (9) and S (1) of chelating molecules ($\mathbf{L^2}$ and phen), with an angle N (9) Cd (1) S (1) equal to 165.66 (3)°. The Cd (1) -N (9) and Cd (1) -S (1) distances are 2.449 (1) Å and 2.5778 (4) Å, respectively. When comparing the Cd -N bond lengths of the equatorial N (4), N (8), and N (10) atoms equal to 2.839 (1), 2.314 (1), and 2.362 (1) Å, respectively, the distance Cd (1)-N (4) is very different. This difference is due to the formation of the $\mathbf{L^2}$ ligand with the cadmium cation of a four-membered chelate ring. The chelate angle N (4) Cd (1) S (1) is 59.98°, and in order to weaken the stress in the cycle, the nitrogen atom N (4) in the equatorial position is located more distant from the cadmium atom, thus completing the sixth coordination [5+1] of octahedron.

The Cd - N_{phen} and Cd -S distances are 2.449 (1) Å, 2.362 (1) Å and 2.578 (4) Å, 2.566 (5) Å, respectively, and are close to similar distances in related cadmium complexes with 1-(4-carboxyphenyl)-5-mercapto-1H-tetrazole ligands [20]. Molecule (**V**) is centrosymmetric and contains an eight-membered cycle (-S - C═N → Cd - S - C═N → Cd) in the "chair" conformation; the center of the inversion is in the center of the eight-membered cycle and coincides with the crystallographic center of the inversion. The Cd (1) -Cd (1^i) distance in the cycle is 4.780 (4) Å. The each polymeric chain is stabilized by intramolecular C—H···S bonding. The neighbouring polymeric chains are interlinked through C—H···N, C—H···O and C—H···S bonding to form the 3D network.

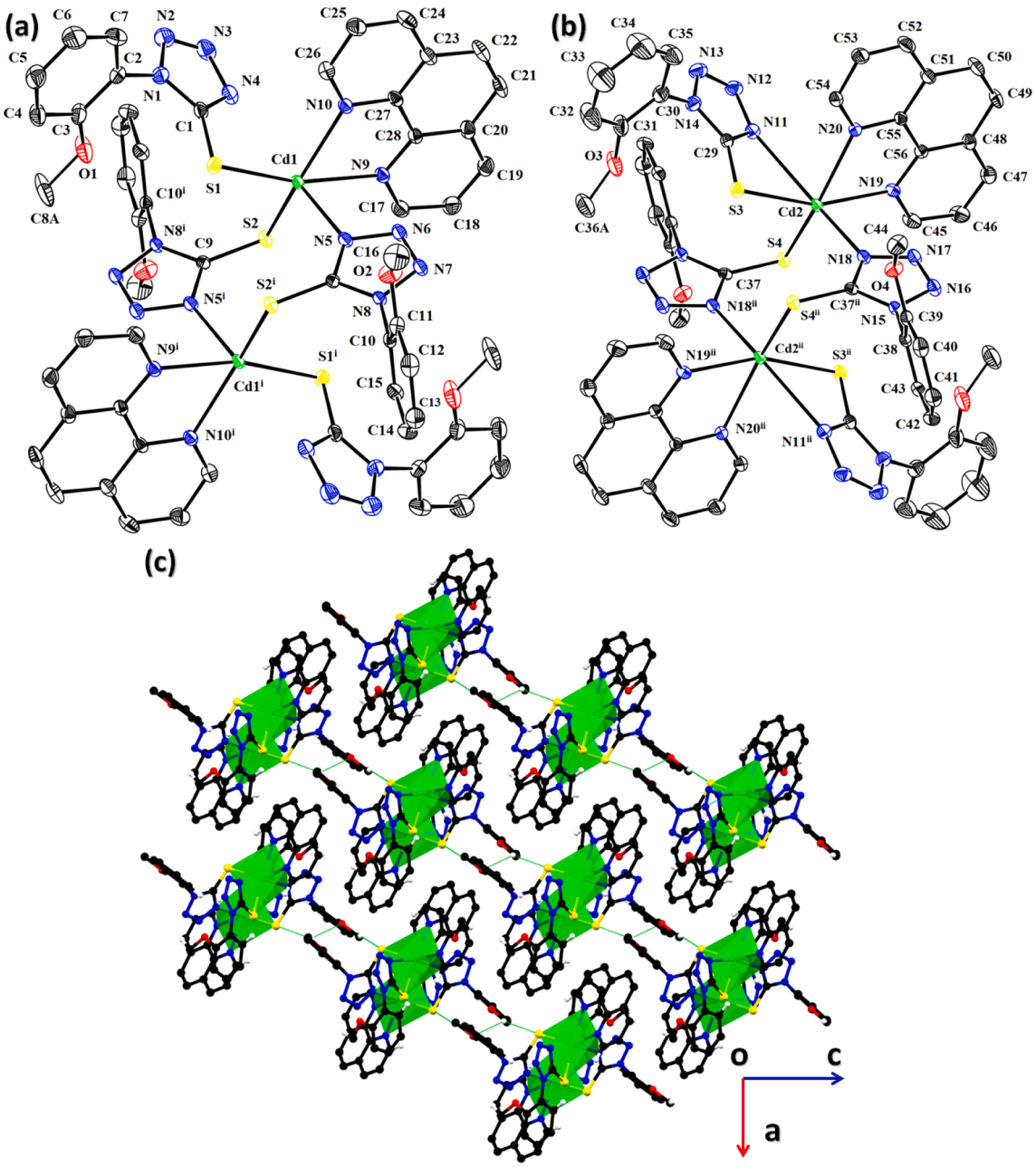

Fig. 5. ORTEP diagram of polymer complex **V** for **(a)** molecule **I**, **(b)** molecule **II** that are drawn at probability level of 50%. H-atoms are not shown for clarity. **(c)** Packing diagram of polymer complex **V** that shows the interlinkage of polymer chains through H-bonding. Selected H-atoms are shown for clarity.

Hirshfeld surface analysis

The non-covalent interactions are the key aspects to understand the supramoelcular behavior of the single crystals. The properties of the single crystals mainly depend on the non-covalent interactions in the single crystals. Crystal explorer 21.5 is used to investigate the non-covalent interactions in the complexes through Hirshfeld surface analysis [23,24]. Hirshfeld surface emerges from an attempt to divide the crystal electron density into molecular fragments for the integration purpose. Numerous important information about the non-covalent interactions can be extracted from the Hirshfeld surface (HS). For example, Hirshfeld surface plotted over normalized distances (dnorm) provides a unique knowledge about the short contacts or H-bonding interactions. Red, white and blue spots stand for the contacts with distance less than, equal and greater than the sum of the Van der Waal radii of the atoms involved [25–34]. Fig. 6(a-d) shows HS plotted over dnorm for complexes **I-III/V**, respectively. In compounds **I-III**, we choose the asymmetric unit for the HS. In present case, the asymmetric unit is not a complete molecule, so the red spots on the HS around metal center and (S/O) atom indicate their involvement in completing the coordination sphere. The short contacts of the intermolecular interactions are visible on the HS by comparatively lighter red spots. For all four compounds, the red spots on the HS except the red spots around metal atom and the symmetry related coordinating (S/O) atoms indicates the short contacts

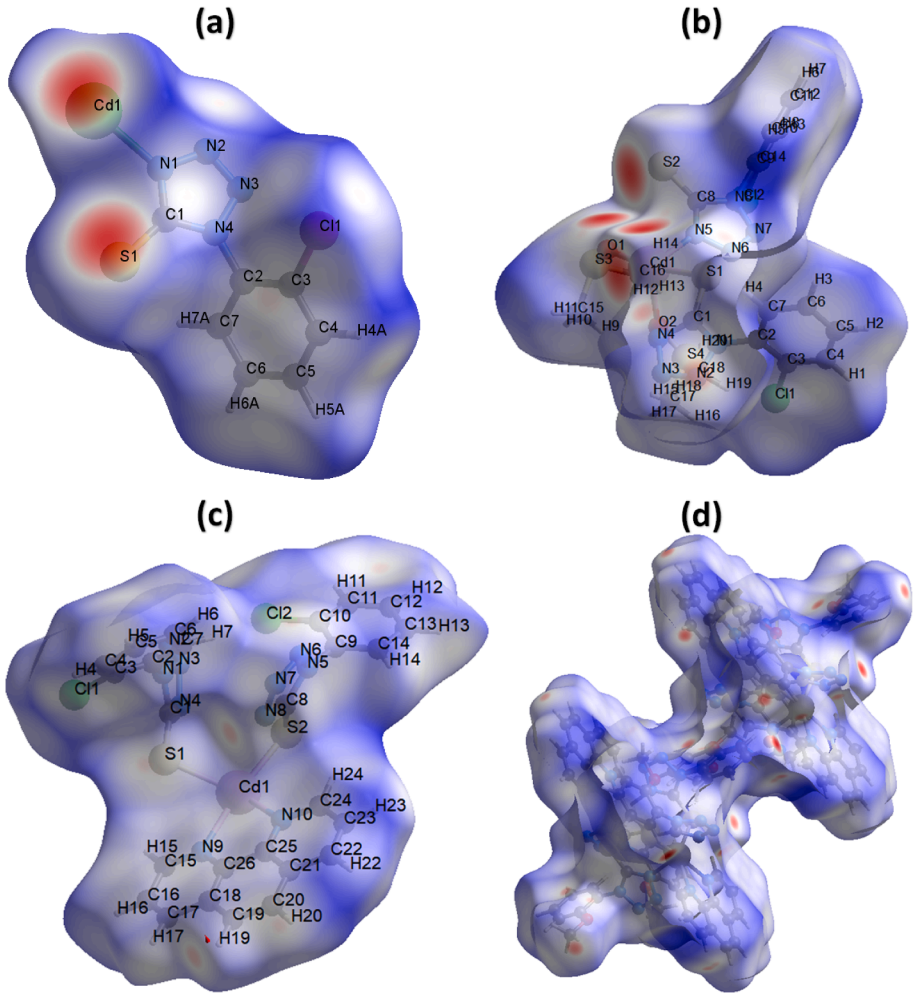

Fig. 6. Hirshfeld surface plotted over dnorm for **(a) I** in the range −0.581 to 1.264 a.u., **(b) II** in the range −0.4629 to 1.8890 a.u., **(c) III** in the range −0.5175 to 1.6067 a.u, **(d) V** in the range −0.2430 to 1.7167 a.u.

that are suitable or good enough to form H-bonding interactions. In addition to provide useful information about the H-bonding interactions, Hirshfeld surfaces are also used in order to recognize interactions weaker than H-bonding specially π···π interactions [27,31,35]. The red and blue spots on the Hirshfeld surface plotted over shape index around the rings indicate their involvement in π···π interactions. Such regions are present on the Hirshfeld surface for compound **I-III/V** (Fig. 7) indicate that π···π interactions are present in them.

2 D finger printing is a used to show the contribution of each short and comparatively longer contacts in the crystal packing [36–43]. While keeping in view the above background, we preformed 2D finger print plots analysis of complexes **I-III/V**. Fig. 8a shows the 2D plot for overall interactions in case of complex **I** containing number of large spikes. The large spikes on it represents the contacts that are important in the understanding of the crystal packing. Cl—H and N—H contacts are the most important contacts for complex **I** with percentage contribution of 15.4 %. The portion of Hirshfeld surface that represent Cl-H and N—H contacts are shown by Fig. 8d and e, respectively by blue region. The H-atoms present nearer to the S-atoms are engaged in short S—H contacts as compare to H-atoms that are at the comparatively larger distance for the S-atom (Fig. 8f). Cd-S and C—H contacts, their contribution in the crystal packing along with their Hirshfeld surfaces are also shown in Fig. 8. The other contacts have very small contribution in the crystal packing as their importance is relatively small. Figs. S2a, S3a and S4a show the 2D finger print plot of overall interactions for complexes **II, III** and **V**, respectively. As it can be seen that the shape of 2 D plots of overall interactions is not same in complexes **I-III/V** which indicate that the contribution of the contacts in the crystal packing of **I-III/V** is different from one another. For complexes **I-III/V**, the H—H contact is the most significant contributor in defining the crystal packing with percentage contribution of 27.6 %, 27.7 % and 37.2 %, respectively. The contribution of H—H contacts in complex **V** is larger than in complex **II** and **III** as the Hirshfeld surface of complex **V** contains larger than H-atoms as compare to the Hirshfeld surface of complexes **II** and **III**. N—H contacts are the second important contact in complex **II** and **III** whereas in complex V, the second important contact is C—H. The 2D plots of other important contacts along with their Hirshfeld surface are shown in Figs. 8, S2, S3 and S4 for complexes **I-III/V**, respectively. The contacts with contribution in the crystal packing greater than 0.9 % except the first five most important contacts for complex **I-III/V** are shown in Fig. 9. H—H contact is the minor contributor in the crystal packing for complex **I** whereas for complexes **II/III/V**, H—H contact has major

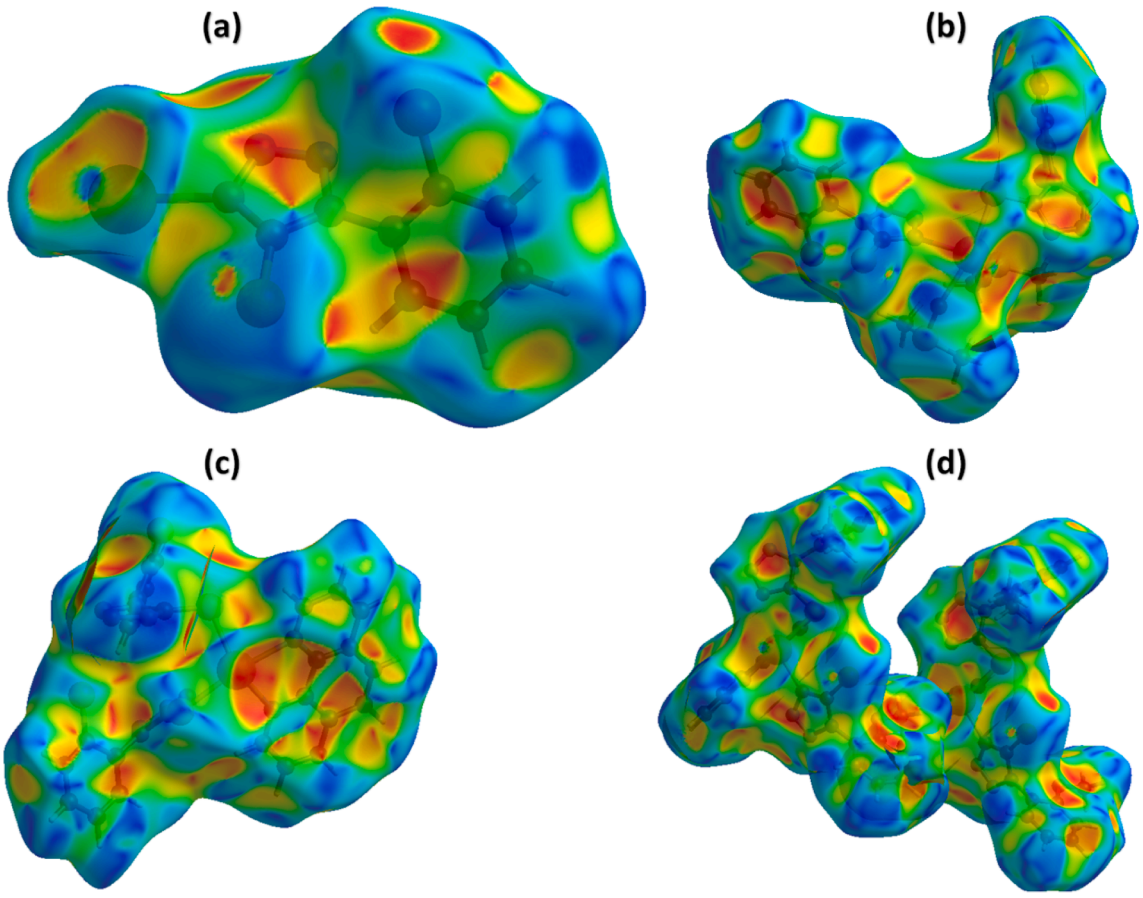

Fig. 7. Hirshfeld surface plotted over shape index in the range −1 to 1 a.u., for **(a) I, (b) II, (c) III, (d) V.**

contribution in the crystal packing. The C—C contact has greater contribution in the crystal packing of complex **III** as compared to in complex **I, II** and **V** which inferred that the interactions involving aromatic rings such as π···π interactions are stronger in complex **III** as compare to in complex **I, II** and **V**. The Cd-S contact has contribution of 10.5 % and 2.3 % in the crystal packing of complex **I** and **II**, respectively whereas for complex **III** and **V**, this contact has contribution less than 0.9 %.

Enrichment ratio provides the propensity or the tendency of the interatomic contact (X, Y) to form crystal packing interactions. It is obtained by diving the proportion of the actual contact in the crystal packing to the theoretical proportion of the random contact. The actual contact is acquired from the Hirshfeld surface analysis. The contacts with enrichment ratio greater than one have higher tendency to form crystal packing interactions as compare to other contacts. For complex **I**, the contact having highest propensity to form crystal packing interactions is Cd-S with enrichment ratio 4.07. In addition to Cd-S contacts, Cl—H, Cd—N, N—H, S—H and N—N contacts have higher tendency to form crystal packing interactions as compare to other contacts with enrichment ratio 3.58, 2.14, 1.25, 1.24 and 1.22, respectively (Table 4). For complex **II**, the contacts that have higher propensity to form crystal packing interactions as compare to other contacts are Cl—S, N—H, Cl—H, C—H and S—H with enrichment ratio 1.97, 1.61, 1.39, 1.23 and 1.11, respectively (Table S1). For complex **III**, the contacts that have higher propensity to form crystal packing interactions as compare to other contacts are, C—C, Cl—H, S—H and Cl—C with enrichment ratio 2.17, 1.47, 1.46 and 1.26, respectively (Table S2). For complex **V**, the contacts that have higher propensity to form crystal packing interactions as compare to other contacts are, C—C, O—H and N—H with enrichment ratio 1.68, 1.57 and 1.50, respectively (Table S3).

The properties of the single crystals depend on how the molecules are packed and how much strongly they interact with each other. If the crystal packing is strong, then it can bear a significant amount of the applied force or stress. In this prospective, we explored the void analysis of the complexes **I-III/V**. Void analysis id carried out using the Hartree-Fock theory (Fig. 10). All the atoms are assumed to be spherically symmetric and electron density of all the atoms are added up to calculate the voids [44]. The volume void is 211.68, 202.55, 148.88 and 403.46 $Å^3$ in complexes **I-III/V**, respectively. The void in the crystal packing of complexes **I-III/V** are 11.4 %, 14.8 %, 10.8 % and 13.8 %, respectively which indicates that there is no large cavity in the crystal packing of complexes **I-III/V**.

UV–vis spectra

In the electronic spectra of complexes (**I/IV**), the maximum of the absorption band in the region of 202.6 nm, which is present in the spectra of ligands $\mathbf{HL^1}$ and $\mathbf{HL^2}$, is shifted to the short-wavelength part of the spectrum, which is typical for transitions associated with charge transfer in ligands $\mathbf{HL^1}$ and $\mathbf{HL^2}$. However, there are no transitions due to

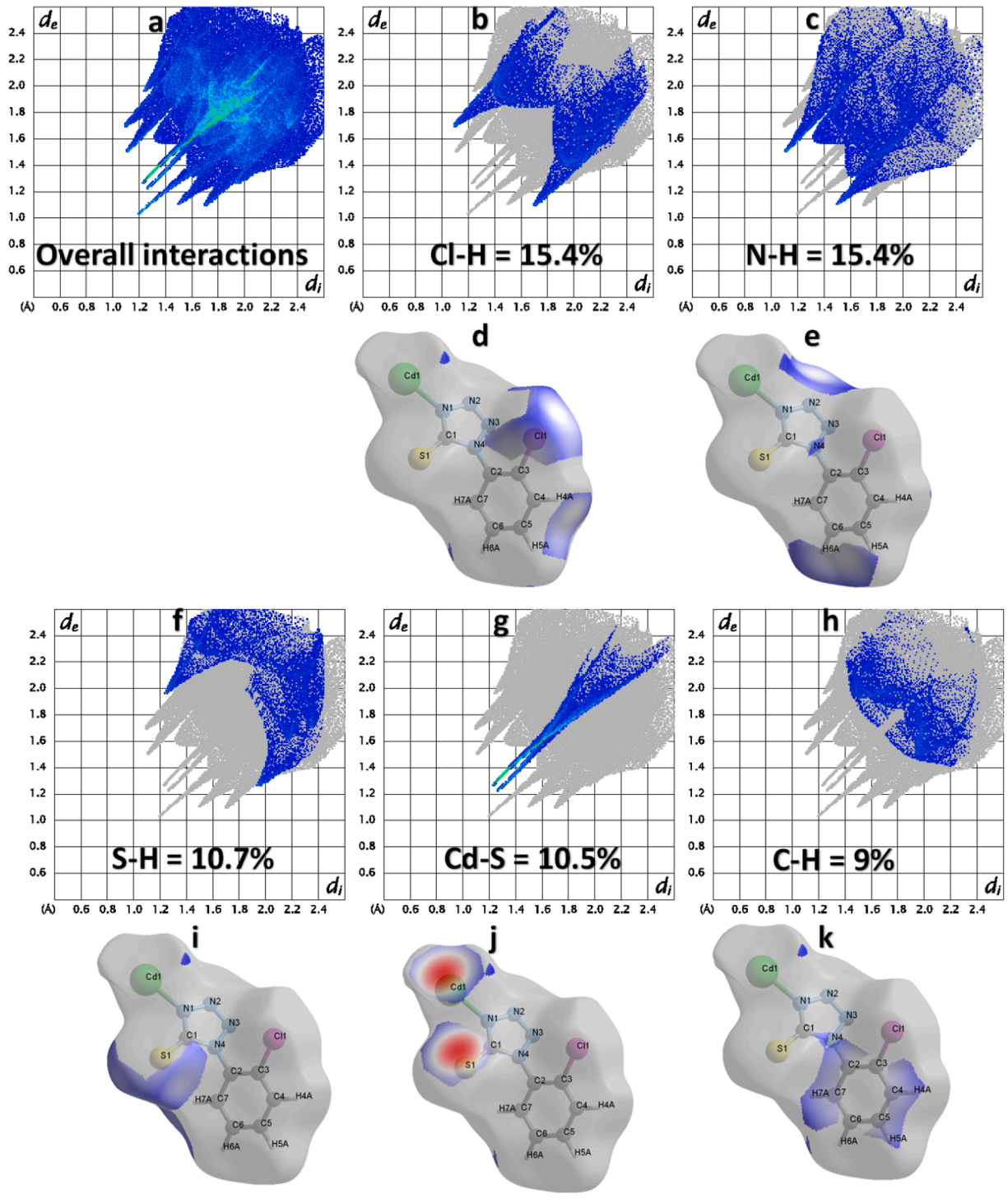

Fig. 8. 2D finger print lot for the overall interactions and for important interatomic contacts with Hirshfeld surface part in **I**.

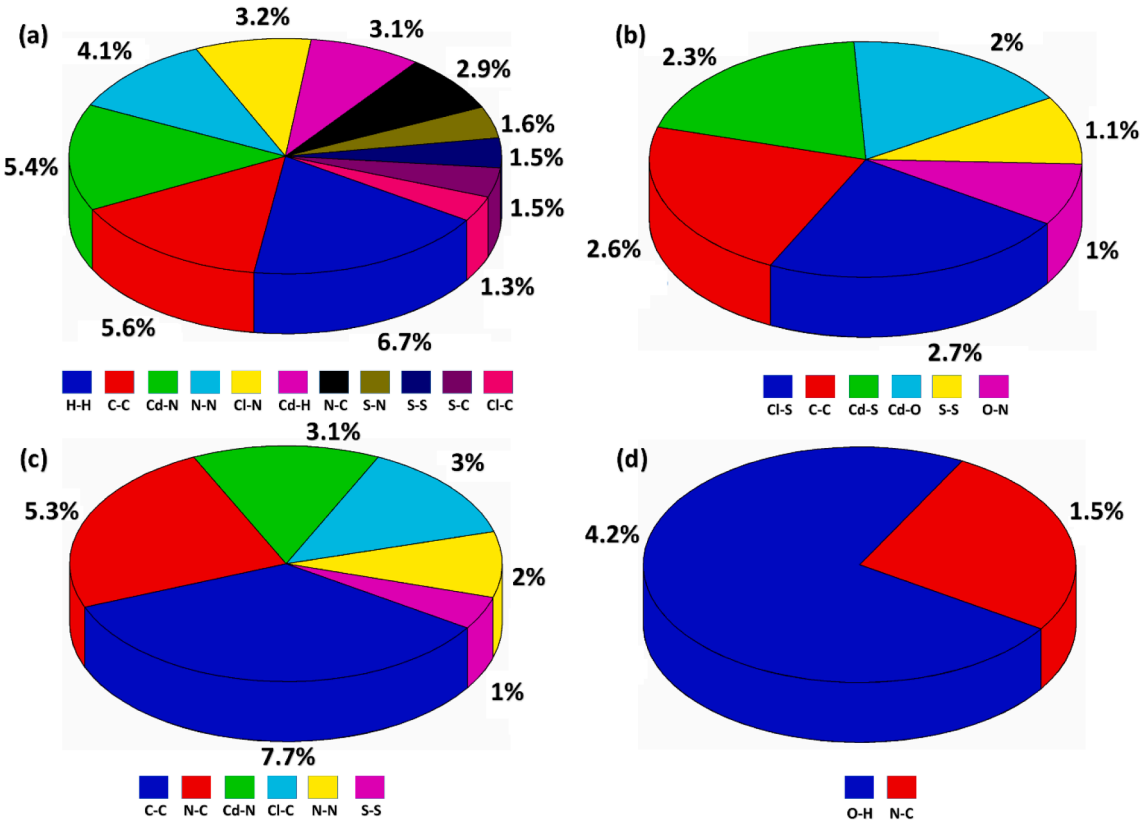

Fig. 9. Graphical representation of the contacts with contribution in the crystal packing greater than 0.9% except for the first five most important contacts for **(a) I, (b) II, (c) III, (d) V**.

Table 4
Enrichment ratio of the pair of chemical species in complex **I**. Enrichment ratio of the pair of the chemical species for which random contact is less than 0.9% is not calculated.

Contact %	Atom	H	C	N	S	Cl	Cd
	H	6.7	9	15.4	10.7	15.4	3.1
	C	9	5.6	2.9		1.3	0.6
	N	15.4	2.9	4.1	1.6	3.2	5.4
	S	10.7		1.6	1.5		10.5
	Cl	15.4	1.3	3.2		0.8	
	Cd	3.1	0.6	5.4	10.5		0.2
Surface%		33.5	12.5	18.35	12.9	10.75	10
Random Contacts %	**Atom**	**H**	**C**	**N**	**S**	**Cl**	**Cd**
	H	11.22					
	C	8.38	1.56				
	N	12.29	4.59	3.37			
	S	8.64	3.23	4.73	1.66		
	Cl	7.20	2.69	3.95	2.77	1.16	
	Cd	6.70	2.50	3.67	2.58	1.08	1.00
Enrichment ratio	**Atom**	**H**	**C**	**N**	**S**	**Cl**	**Cd**
	H	0.60					
	C	1.07	3.58				
	N	1.25	0.63	1.22			
	S	1.24	0.00	0.34	0.90		
	Cl	2.14	0.48	0.81	0.00	0.69	
	Cd	0.46	0.24	1.47	4.07	0.00	0.20

the ligand field, which should appear in the visible region of the spectrum. In solutions of complexes **III** and **V**, weak intermolecular interactions occur, mainly due to the second ligand (o-phenanthroline). Compared to the spectrum of pure o-phenanthroline, the spectra of complexes **III** and **V** show a slight bathochromic shift from 264 nm to 265.6 nm in complex **V** and up to 268.6 nm in complex **III**. Complex **III** also exhibits a hypsochromic shift of the 230.2 nm band to 225.4 nm.

Results of studying the bactericidal activity of the compounds

The antimicrobial activity of the synthesized compounds (**HL^1**, **HL^2**, **I, IV**) was studied (Table 5). Compounds (**I, IV**) were found to possess bactericidal activity. The starting ligands (**HL^1**, **HL^2**) are not bactericidal. The antibacterial activities of the complexes are probably due to their stability, as a result of which they have more free ions in solution which enhances the cooperative interaction between the metal ions and the ligand and involves the formation of a hydrogen bond through the nitrogen or sulfur atom in the complexes with the active centers of the cell constituents, resulting in interference with the normal cell process. The chelation tends to make the complex act as more powerful and potent bacterial agents, thus killing more bacteria than the ligand. The chelation increases the lipophilic character of the metal chelate compound and favors its permeation through the lipoid layers of the bacterial membranes and thus retards the normal cell processes.

Theoretical study

The interaction energy between the molecular pairs provide a vital information about the crystal packing environment in the single crystals. In this prospective, we are going to explore the interaction energy between molecular pairs and energy frameworks for the non-polymeric crystal structures (**II/III/V**). The interaction energy between molecular pairs is the sum of four types of energies named as electrostatic coulomb energy (E_{ele}), polarization energy (E_{pol}), dispersion energy (E_{dis}) and repulsive energy (E_{rep}) [45]. Electrostatic energy between molecular pairs can be attractive or repulsive whereas dispersion and

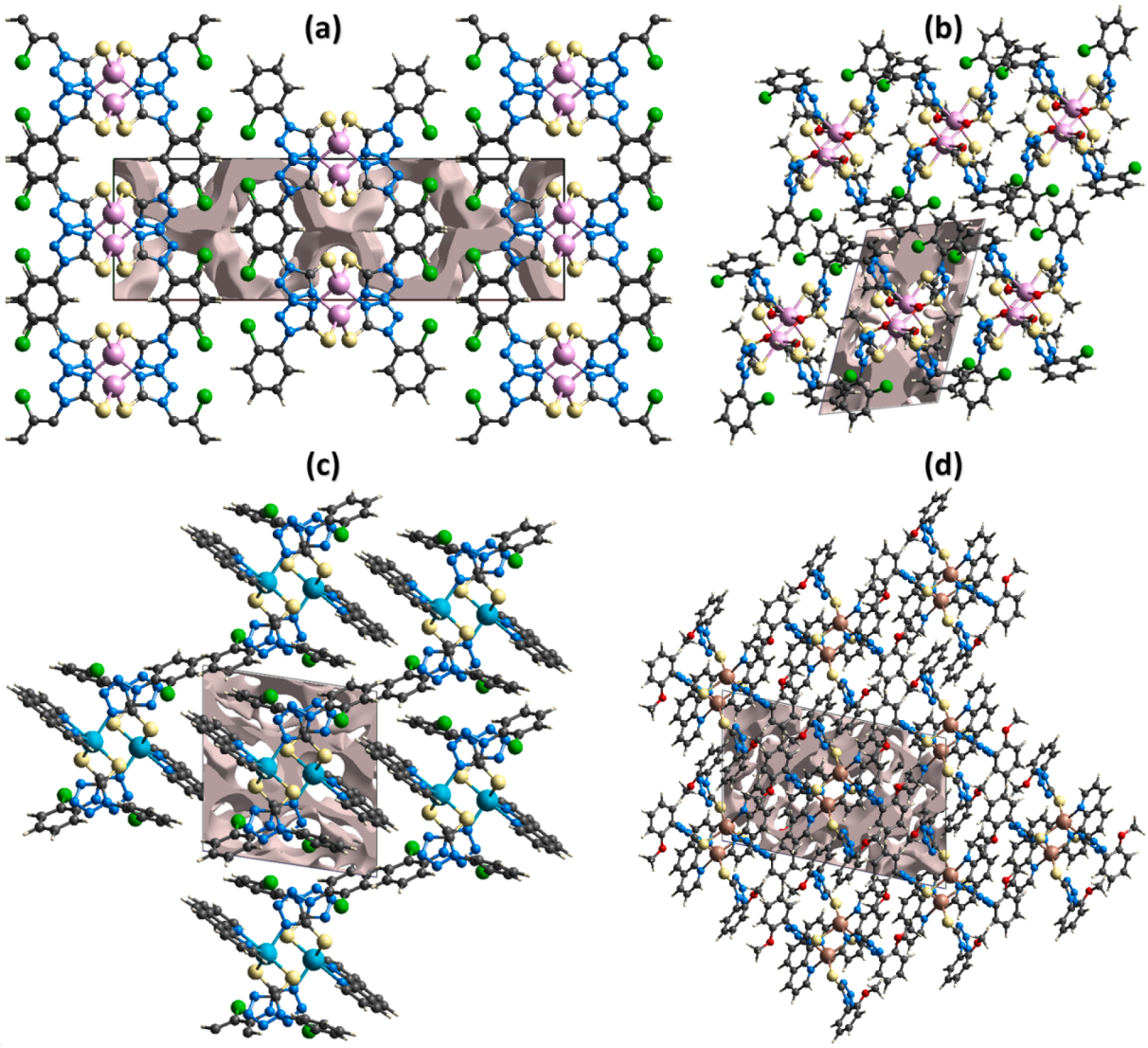

Fig. 10. Graphical view of voids in the crystal packing of **(a) I, (b) II, (c) III, (d) V.**

Table 5
Bactericidal effect of 1% solutions compounds (**HL^1, HL^2, I, IV**) in DMSO.

Compound	*Staphylococcus aureus*		*Escherichia coli*	
	D zones of growth inhibition, mm (ignoring well diameter)	characteristic of bactericidity	D zones of growth inhibition, mm (ignoring well diameter)	characteristic of bactericidity
HL^1	1	Nonbactericidal	0	Nonbactericidal
HL^2	3	Nonbactericidal	2	Nonbactericidal
I	18	Bactericidal	20	Strongly bactericidal
IV	10	Bactericidal	10	Bactericidal

polarization energies are always attractive. The electrostatic energy and dispersion energy are the major contributor in defining the total interaction energy between molecular pairs. Fig. 11(a-f) shows the energy frame works of electrostatic and dispersion energy for complex **II/III/V**. The width of the cylinder that connects the molecular centers is directly proportional to the strength of the interaction energy. For complex **II**, the width of cylinder for electrostatic and dispersion energy is almost equal which inferred that the contribution of both energies in defining the total energy is almost same. This is also clear from Fig. 11g which showed that for complex **II**, the percentage contribution of electrostatic and dispersion energy is 40.2 % and 43.7 %, respectively. The situation is quite different in case of complex **III** and **V**. In complex **III** and **V**, the contribution of dispersion energy is significantly larger than the contribution of the electrostatic energy. Total attractive energy among the molecular pairs is greatest for complex **II** (−257.6 kJ/mol) and smallest for complex **III** (−50.5 kJ/mol).

Conclusion

In the current research work, we explored the synthesis of cadmium complexes (**I-V**) containing heterocyclic ligands. The synthesized compounds are characterized by ^{1}H, ^{13}C NMR, UV–vis spectroscopy and elemental analysis. Furthermore, the single crystal of the complexes **I-III/V** are characterized by X-rays diffraction technique. The supramolecular assembly of the complexes **I-III/V** is explored by Hirshfeld surface analysis in order to elaborate the non-covalent interactions. Enrichment ratio is computed for all the possible pair of chemical species in complexes **I-III/V** which inferred that Cd-S, Cd-S are the contacts of highest propensity of form the crystal packing interactions in complex **I** and **II**, respectively whereas C—C contact has the highest propensity in

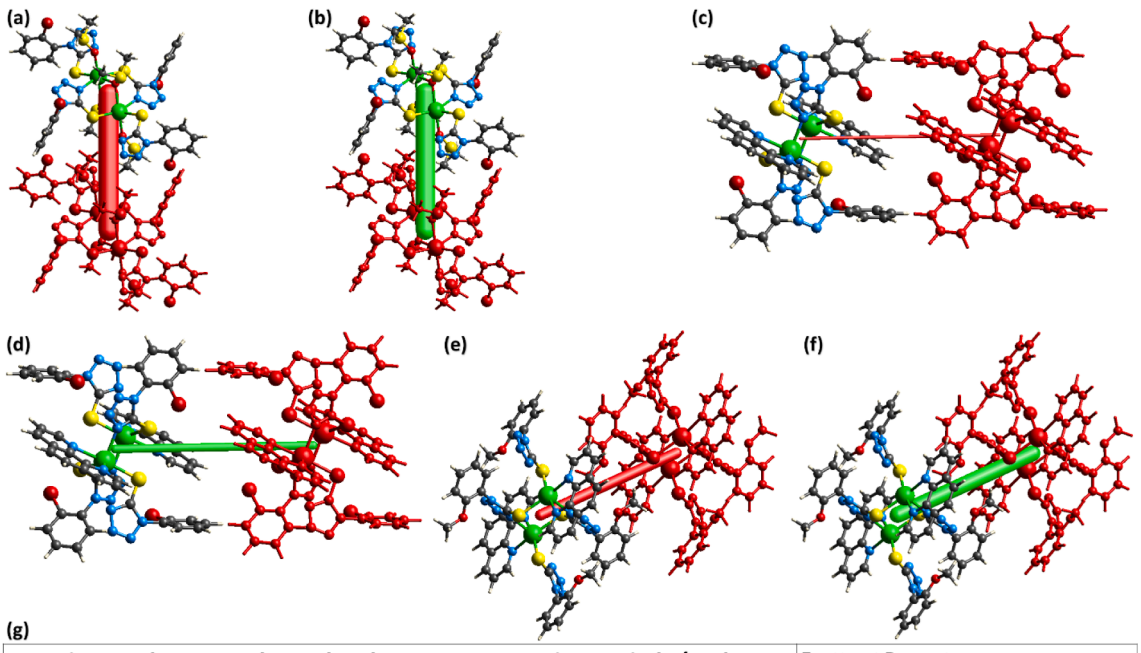

(g)

R = Distance between the molecular centers. Energies are in kJ/mol							E_attract Percentage		
R	E_ele	E_pol	E_dis	E_rep	E_tot	E_attract	E_ele %	E_pol %	E_dis %
Complex II									
11.45	-103.5	-41.7	-112.4	83.8	-165.9	-257.6	40.2	16.2	43.7
Complex III									
12.88	-12.7	-5.5	-37.7	0.0	-50.5	-50.5	25.1	10.9	74.6
Complex V									
11.31	-49.6	-20.7	-82.1	61.8	-87.9	-152.4	32.5	13.6	53.9
Scale factors for benchmarked energy model (CE-HF ... HF/3-21G electron densities)									
k_ele = 1.019		k_pol = 0.651		k_dis = 0.901				k_rep = 0.811	

Fig. 11. Energy framework for coulomb electrostatic energy for complex **(a) II**, **(c) III**, **(e) V**. Energy framework for dispersion energy for complex **(b) II**, **(d) III**, **(f) V**. **(g)** Summary of the interaction energy results for complex **II/III/V**.

case of complex **III** and **V**. Void analysis conformed that the molecules are strongly packed in complexes **I-III** and **V**. The interaction energy between molecular pairs and energy frameworks for non-polymeric crystal structures (**II/III/V**) specify the role of various kinds of interaction energies in stabilization of the crystal packing. The compounds **I** and **IV** showed bactericidal activity against *Staphylococcus aureus* and *Escherichia coli*.

Declaration of Competing Interest

The authors declare that they have no known competing financial interests or personal relationships that could have appeared to influence the work reported in this paper.

Data availability

The crystallographic data is submitted on CCDC website and will be available free of charge.

Acknowledgments

The X-ray study has been performed in the framework of the Russian state assignment using an equipment of the Analytical Center of the G.A. Razuvaev IOMC RAS. This work was supported by the RUDN University Strategic Academic Leadership Program *Priority-2030*. The work was carried out using the equipment of the Center for Collective Use "New Materials and Resource Saving Technologies" (Nizhny Novgorod State University named after N.I. Lobachevsky).

Appendix A. Supplementary data

Supplementary data to this article can be found online at https://doi.org/10.1016/j.rechem.2022.100600.

References

[1] E.D. Shtefan, V.Y. Vvedenskii, The tautomerism of heterocyclic thiols. Five-membered heterocycles, Russ. Chem. Rev. 65 (4) (1996) 307–314.
[2] R. Askerov, A. Maharramov, V. Osmanov, E. Baranov, G. Borisova, P. Dorovatovskii, V. Khrustalev, A. Borisov, Molecular and crystal structure of 1-(4-fluorophenyl)-1, 4-dihydro-1H-tetrazole-5-thione and its complex with cadmium (II), J. Struct. Chem. 59 (7) (2018) 1658–1663.
[3] R. Askerov, A. Magerramov, V. Osmanov, E. Baranov, G. Borisova, A. Samsonova, A. Borisov, 1-(2-Methoxyphenyl)-1, 4-dihydro-5H-tetrazole-5-thione and its complex with Cd (II): molecular and crystal structures, Russ. J. Coord. Chem. 45 (2) (2019) 112–118.
[4] R.K. Askerov, A.M. Maharramov, A.N. Khalilov, M. Akkurt, A.A. Akobirshoeva, V. Osmanov, A. Borisov, Crystal structure and Hirshfeld surface analysis of 1-(2-fluorophenyl)-1H-tetrazole-5 (4H)-thione, Acta Crystallogr. E: Crystallogr. Commun. 76 (7) (2020) 1007–1011.
[5] J.-F. Song, J. Wang, S.-Z. Li, Y. Li, R.-S. Zhou, Five new complexes based on 1-phenyl-1H-tetrazole-5-thiol: Synthesis, structural characterization and properties, J. Mol. Struct. 1129 (2017) 1–7.
[6] M. Hernández-Arganis, M. Moya-Cabrera, V. Jancik, D. Martínez-Otero, A. M. Cotero-Villegas, M. del Carmen Pérez-Redondo, R. Cea-Olivares, Synthesis and structural study of alkali metal complexes derived from 1-phenyl-tetrazole-thiolate and crown ethers, Inorg. Chim. Acta 475 (2018) 83–89.

[7] M. Hernández-Arganis, R.A. Toscano, M. Moya-Cabrera, V. García-Montalvo, R. Cea-Olivares, Structural study of alkaline 1-phenyl-1H-1,2,3,4-tetrazole-5-thiolate salts: an example of periodicity in alkaline cations, Z. Anorg. Allg. Chem. 630 (11) (2004) 1627–1631.

[8] M. Imran, A. Mix, B. Neumann, H.-G. Stammler, U. Monkowius, P. Bleckenwegner, N.W. Mitzel, Boron-centered soft ligands based on tetrazole units and their complexes with sodium, potassium and bismuth ions, Dalton Trans. 43 (39) (2014) 14737–14748.

[9] Y. Li, C.-Q. Wang, H.-D. Bian, F.-P. Huang, H. Liang, Q. Yu, Three CoII/CoIII complexes with a 1-substituted tetrazole-5-thiol ligand, J. Coord. Chem. 65 (20) (2012) 3665–3673.

[10] A. Ilie, C.I. Rat, S. Scheutzow, C. Kiske, K. Lux, T.M. Klapötke, C. Silvestru, K. Karaghiosoff, Metallophilic bonding and agostic interactions in gold (I) and silver (I) complexes bearing a thiotetrazole unit, Inorg. Chem. 50 (6) (2011) 2675–2684.

[11] N.A. Sanina, G.I. Kozub, T.A. Kondrat'eva, G.V. Shilov, D.V. Korchagin, N. S. Emel'yanova, O.K. Poleshchuk, A.V. Chernyak, A.V. Kulikov, F.B. Mushenok, N. S. Ovanesyan, S.M. Aldoshin, Structure and properties of bis (1-phenyl-1h-tetrazole-5-thiolate) diiron tetranitrosyl, J. Mol. Struct. 1041 (2013) 183–189.

[12] M. Bharty, R. Dani, S. Kushawaha, N. Singh, R. Kharwar, R. Butcher, Mn (II), Ni (II), Cu (II), Zn (II), Cd (II), Hg (II) and Co (II) complexes of 1-phenyl-1H-tetrazole-5-thiol: Synthesis, spectral, structural characterization and thermal studies, Polyhedron 88 (2015) 208–221.

[13] M. Taheriha, M. Ghadermazi, V. Amani, Dimeric and polymeric mercury (II) complexes of 1-methyl-1, 2, 3, 4-tetrazole-5-thiol: Synthesis, crystal structure, spectroscopic characterization, and thermal analyses, J. Mol. Struct. 1107 (2016) 57–65.

[14] A.W. Addison, T.N. Rao, J. Reedijk, J. van Rijn, G.C. Verschoor, Synthesis, structure, and spectroscopic properties of copper (II) compounds containing nitrogen–sulphur donor ligands; the crystal and molecular structure of aqua [1,7-bis (N-methylbenzimidazol-2′-yl)-2,6-dithiaheptane] copper (II) perchlorate, J. Chem. Soc., Dalton trans. 7 (1984) 1349–1356.

[15] R.K. Askerov, Y. El Bakri, V.K. Osmanov, S. Ahmad, K. Saravanan, G.N. Borisova, R. H. oglu Nazarov, E.V. Baranov, G.K. Fukin, D.G. Fukina, Complexes of 1-(2-R (F, CH3, Cl)-phenyl)-1,4-dihydro-5H-tetrazole-5-thiones with cadmium chloride: Synthesis, molecular, crystal structures and computational investigation approach, J. Inorg. Biochem. 231 (2022) 111791.

[16] R. Askerov, V. Osmanov, O. Kovaleva, E. Baranov, G. Fukin, D. Fukina, A. Boryakov, A. Magerramov, A. Borisov, Complexes of 1-(4-methoxyphenyl)-1, 4-dihydro-5H-tetrazole-5-thione and 1-(2-methoxyphenyl)-1,4-dihydro-5H-tetrazole-5-thione with cadmium chloride: synthesis and molecular and crystal structures, Russ. J. Coord. Chem. 47 (11) (2021) 741–750.

[17] S.S. Hasanova, L.N. Mamedova, M. Ashfaq, K.S. Munawar, E.M. Movsumov, M. Khalid, M.N. Tahir, M. Imran, Synthesis, crystal structure, Hirshfeld surface analysis and theoretical investigation of polynuclear coordination polymers of cobalt and manganese complexes with nitrobenzene and pyrazine, J. Mol. Struct. 1250 (2022) 131851.

[18] H. Raza, I. Yildiz, F. Yasmeen, K.S. Munawar, M. Ashfaq, M. Abbas, M. Ahmed, H. A. Younus, S. Zhang, N. Ahmad, Synthesis of a 2D copper (II)-carboxylate framework having ultrafast adsorption of organic dyes, J. Colloid Interface Sci. 602 (2021) 43–54.

[19] H. Kargar, M. Fallah-Mehrjardi, R. Behjatmanesh-Ardakani, M.N. Tahir, M. Ashfaq, K.S. Munawar, Synthesis, crystal structure determination, Hirshfeld surface analysis, spectral characterization, theoretical and computational studies of titanium (IV) Schiff base complex, J. Coord. Chem. 74 (16) (2021) 2682–2700.

[20] K.S. Ali, M. Ashfaq, M.N. Tahir, E.M. Movsumov, K.S. Munawar, Synthesis, crystal structure, Hirshfeld surface and void analysis of bis (μ_2-4-aminobenzoato-κ^2O:O′) bis [bis (4-aminobenzoato-κ^2O,O′) diaquathulium (III)] dihydrate, Acta Crystallogr. E: Crystallogr. Commun. 78 (3) (2022) 282–286.

[21] H. Kargar, M. Ashfaq, M. Fallah-Mehrjardi, R. Behjatmanesh-Ardakani, K. S. Munawar, M.N. Tahir, Theoretical studies, Hirshfeld surface analysis, and crystal structure determination of a newly synthesized benzothiazole copper (II) complex, J. Mol. Struct. 1261 (2022) 132905.

[22] H. Kargar, M. Ashfaq, M. Fallah-Mehrjardi, R. Behjatmanesh-Ardakani, K. S. Munawar, M.N. Tahir, Synthesis, crystal structure, spectral characterization, theoretical and computational studies of Ni (II), Cu (II) and Zn (II) complexes incorporating Schiff base ligand derived from 4-(diethylamino) salicylaldehyde, Inorg. Chim. Acta 536 (2022) 120878.

[23] P.R. Spackman, M.J. Turner, J.J. McKinnon, S.K. Wolff, D.J. Grimwood, D. Jayatilaka, M.A. Spackman, CrystalExplorer: A program for Hirshfeld surface analysis, visualization and quantitative analysis of molecular crystals, J. Appl. Crystallogr. 54 (3) (2021) 1006–1011.

[24] J.J. McKinnon, A.S. Mitchell, M.A. Spackman, Hirshfeld surfaces: a new tool for visualising and exploring molecular crystals, Chem. Eur. J. 4 (11) (1998) 2136–2141.

[25] M.A. Spackman, D. Jayatilaka, Hirshfeld surface analysis, CrystEngComm 11 (1) (2009) 19–32.

[26] M.N. Tahir, M. Ashfaq, F. Alexander, J. Caballero, E.W. Hernández-Rodríguez, A. Ali, Rationalizing the stability and interactions of 2, 4-diamino-5-(4-chlorophenyl)-6-ethylpyrimidin-1-ium 2-hydroxy-3,5-dinitrobenzoate salt, J. Mol. Struct. 1193 (2019) 185–194.

[27] M. Haroon, T. Akhtar, M. Yousuf, M.N. Tahir, L. Rasheed, S.S. Zahra, M. Ashfaq, Synthesis, crystal structure, Hirshfeld surface investigation and comparative DFT studies of ethyl 2-[2-(2-nitrobenzylidene) hydrazinyl] thiazole-4-carboxylate, BMC. Chem. 16 (1) (2022) 1–17.

[28] A. Ali, M. Khalid, M.F.U. Rehman, S. Haq, A. Ali, M.N. Tahir, M. Ashfaq, F. Rasool, A.A.C. Braga, Efficient synthesis, SC-XRD, and theoretical studies of O-Benzenesulfonylated pyrimidines: Role of noncovalent interaction influence in their supramolecular network, ACS omega 5 (25) (2020) 15115–15128.

[29] A. Ali, M. Khalid, M.N. Tahir, M. Imran, M. Ashfaq, R. Hussain, M.A. Assiri, I. Khan, Synthesis of diaminopyrimidine sulfonate derivatives and exploration of their structural and quantum chemical insights via SC-XRD and the DFT approach, ACS omega 6 (10) (2021) 7047–7057.

[30] M. Ashfaq, M.N. Tahir, A. Kuznetsov, S.H. Mirza, M. Khalid, A. Ali, DFT and single crystal analysis of the pyrimethamine-based novel co-crystal salt: 2,4-diamino-5-(4-chloro-phenyl)-6-ethylpyrimidin-1-ium: 4-hydroxybenzoate: methanol: hydrate (1:1:1:1)(DEHMH), J. Mol. Struct. 1199 (2020) 127041.

[31] A.N. Malik, A. Kuznetsov, A. Ali, M. Ashfaq, M.N. Tahir, A. Siddique, Imine-based Zwitterion: Synthesis, single-crystal characterization, and computational investigation, J. Mol. Struct. 1253 (2022) 132237.

[32] M.N. Ahmed, M. Madni, S. Anjum, S. Andleeb, S. Hameed, A.M. Khan, M. Ashfaq, M.N. Tahir, D.M. Gil, A. Frontera, Crystal engineering with pyrazolyl-thiazole derivatives: Structure-directing role of π-stacking and σ-hole interactions, CrystEngComm 23 (18) (2021) 3276–3287.

[33] H. Mehmood, M. Khalid, M. Haroon, T. Akhtar, M. Ashfaq, M.N. Tahir, M.U. Khan, M. Imran, A.A.C. Braga, S. Woodward, Synthesis, characterization and DFT calculated properties of electron-rich hydrazinylthiazoles: Experimental and computational synergy, J. Mol. Struct. 1245 (2021) 131043.

[34] M. Ashfaq, K.S. Munawar, M.N. Tahir, N. Dege, M. Yaman, S. Muhammad, S. S. Alarfaji, H. Kargar, M.U. Arshad, Synthesis, crystal structure, Hirshfeld surface analysis, and computational study of a novel organic salt obtained from benzylamine and an acidic component, ACS Omega 6 (34) (2021) 22357–22366.

[35] B.A. Khan, S.S. Hamdani, M.N. Ahmed, S. Hameed, M. Ashfaq, A.M. Shawky, M. A. Ibrahim, P.A. Sidhom, Synthesis, X-ray diffraction analysis, quantum chemical studies and α-amylase inhibition of probenecid derived S-alkylphthalimide-oxadiazole-benzenesulfonamide hybrids, J. Enzyme Inhib. Med. Chem. 37 (1) (2022) 1464–1478.

[36] A. Ali, A. Kuznetsov, M.U. Khan, M.N. Tahir, M. Ashfaq, A.R. Raza, S. Muhammad, 2-Amino-6-methylpyridine based co-crystal salt formation using succinic acid: Single-crystal analysis and computational exploration, J. Mol. Struct. 1230 (2021) 129893.

[37] M. Ashfaq, K.S. Munawar, G. Bogdanov, A. Ali, M.N. Tahir, G. Ahmed, A. Ramalingam, M.M. Alam, M. Imran, S. Sambandam, B. Munir, Single crystal inspection, Hirshfeld surface investigation and DFT study of a novel derivative of 4-fluoroaniline: 4-((4-fluorophenyl)amino)-4-oxobutanoic acid (BFAOB), J. Iran. Chem. Soc. 19 (5) (2022) 1953–1961.

[38] A. Ali, M. Khalid, M. Ashfaq, A.N. Malik, M.N. Tahir, M.A. Assiri, M. Imran, S.F. de AlcântaraMorais, A.A.C. Braga, Preparation, QTAIM and single-crystal exploration of the pyrimethamine-based co-crystal salts with substituted benzoic acids, ChemistrySelect 7 (17) (2022) e202200349.

[39] H. Kargar, M. Fallah-Mehrjardi, M. Ashfaq, K.S. Munawar, M.N. Tahir, R. Behjatmanesh-Ardakani, H. Amiri Rudbari, A. Adabi Ardakani, S. Sedighi-Khavidak, Zn (II) complexes containing O,N,N,O-donor Schiff base ligands: synthesis, crystal structures, spectral investigations, biological activities, theoretical calculations and substitution effect on structures, J. Coord. Chem. 74 (16) (2021) 2720–2740.

[40] J.J. McKinnon, D. Jayatilaka, M.A. Spackman, Towards quantitative analysis of intermolecular interactions with Hirshfeld surfaces, Chem. Commun. 37 (2007) 3814–3816.

[41] M. Ashfaq, G. Bogdanov, V. Glebov, A. Ali, M.N. Tahir, S. Abdullah, Single crystal investigation, Hirshfeld surface analysis and DFT exploration of the pyrimethamine-based novel organic salt: 2, 4-diamino-5-(4-chlorophenyl)-6-ethylpyrimidin-1-ium 3-carboxybenzoate hydrate (1:1:1), J. Mol. Struct. 1224 (2021) 129309.

[42] M. Ashfaq, A. Ali, A. Kuznetsov, M.N. Tahir, M. Khalid, DFT and single-crystal investigation of the pyrimethamine-based novel co-crystal salt: 2,4-diamino-5-(4-chlorophenyl)-6-ethylpyrimidin-1-ium-4-methylbenzoate hydrate (1: 1: 1)(DEMH), J. Mol. Struct. 1228 (2021) 129445.

[43] M. Ashfaq, G. Bogdanov, A. Ali, M.N. Tahir, S. Abdullah, Pyrimethamine-based novel co-crystal salt: synthesis, single-crystal investigation, Hirshfeld surface analysis and DFT inspection of the 2,4-diamino-5-(4-chlorophenyl)-6-ethylpyrimidin-1-ium 2, 4-dichlorobenzoate (1: 1)(DECB), J. Mol. Struct. 1235 (2021) 130215.

[44] M.J. Turner, J.J. McKinnon, D. Jayatilaka, M.A. Spackman, Visualisation and characterisation of voids in crystalline materials, CrystEngComm 13 (6) (2011) 1804–1813.

[45] W.H. Pearson, J.J. Urban, A.H.R. MacArthur, S. Lin, D.W.L. Cabrera, Crystal structures of N-[4-(trifluoromethyl)phenyl]benzamide and N-(4-methoxyphenyl) benzamide at 173 K: a study of the energetics of conformational changes due to crystal packing, Acta Crystallogr. E: Crystallogr. Commun. 78 (3) (2022) 297–305.